Injury 54 (2023) 111080

Contents lists available at ScienceDirect

Injury

journal homepage: www.elsevier.com/locate/injury

Employing direct electromagnetic coupling to assess acute fracture healing: An ovine model assessment

Kevin M. Labus [a], Jakob Wolynski [a], Jeremiah Easley [b], Holly L. Stewart [b], Milan Ilic [c], Branislav Notaros [d], Taylor Zagrocki [a], Christian M. Puttlitz [a], Kirk C. McGilvray [a,*]

[a] Orthopaedic Bioengineering Research Laboratory, Department of Mechanical Engineering, Colorado State University, Fort Collins, CO, USA
[b] Preclinical Surgical Research Laboratory, Department of Clinical Sciences, Colorado State University, Fort Collins, Colorado, USA
[c] University of Belgrade, School of Electrical Engineering, Belgrade, Serbia
[d] Electromagnetic Laboratory, Department of Electrical and Computer Engineering, Colorado State University, Fort Collins, Colorado, USA

ARTICLE INFO

Keywords:
Fracture compliance
Acute fracture healing
Ovine model
Direct electromagnetic coupling (DEC)
Radiographic union score for tibia (mRUST)
Biomechanical monitoring

ABSTRACT

Objectives: This study explored the efficacy of collecting temporal fracture site compliance data via an advanced direct electromagnetic coupling (DEC) system equipped with a Vivaldi-type antenna, novel calibration technique, and multi-antenna setup (termed maDEC) as an approach to monitor acute fracture healing progress in a translational large animal model. The overarching goal of this approach was to provide insights into the acute healing dynamics, offering a promising avenue for optimizing fracture management strategies.
Methods: A sample of twelve sheep, subjected to ostectomies and intramedullary nail fixations, was divided into two groups, simulating normal and impaired healing scenarios. Sequential maDEC compliance or stiffness measurements and radiographs were taken from the surgery until euthanasia at four or eight weeks and were subsequently compared with post-sacrifice biomechanical, micro-CT, and histological findings.
Results: The results showed that the maDEC system offered straightforward quantification of fracture site compliance via a multiantenna array. Notably, the rate of change in the maDEC-measured bending stiffness significantly varied between normal and impaired healing groups during both the 4-week ($p = 0.04$) and 8-week ($p = 0.02$) periods. In contrast, radiographically derived mRUST healing measurements displayed no significant differences between the groups ($p = 0.46$). Moreover, the cumulative normalized stiffness maDEC data significantly correlated with post-sacrifice mechanical strength ($r^2 = 0.80$, $p < 0.001$), micro-CT measurements of bone volume fraction ($r^2 = 0.60$, $p = 0.003$), and density ($r^2 = 0.60$, $p = 0.003$), and histomorphometric measurements of new bone area fraction ($r^2 = 0.61$, $p = 0.003$) and new bone area ($r^2 = 0.60$, $p < 0.001$).
Conclusions: These data indicate that the enhanced maDEC system provides a non-invasive, accurate method to monitor fracture healing during the acute healing phase, showing distinct stiffness profiles between normal and impaired healing groups and offering critical insights into the healing process's progress and efficiency.

Introduction

Despite significant advancements in fracture fixation techniques, nonunion incidences remain common, particularly in long bones such as the tibia. Up to 12 % of tibia fracture cases result in nonunion, leading to a substantial 118 % increase in treatment costs [1,2]. Identifying a nonunion employing prevailing diagnostic standards such as radiographic imaging typically necessitates a period exceeding six months post-fracture [3,4]. Research indicates the considerable benefits of swift identification of abnormal fracture healing. This rapid detection can notably decrease healthcare costs and patient discomfort by enabling improved early-stage clinical management. Promptly deploying suitable secondary interventions and sophisticated treatment techniques can correct the course of healing and enhance patient outcomes [5]. Specifically, detecting nonunions at an early stage allows for the immediate introduction of appropriate secondary interventions. These may include bone grafting, electrical stimulation, low-intensity pulsed ultrasound, or applying FDA-approved pharmaceutical agents [6,7]. Additionally, the negative correlation between clinical outcomes and the time between initial and revision surgeries further highlights the importance of

* Corresponding author.
E-mail address: Kirk.McGilvray@colostate.edu (K.C. McGilvray).

https://doi.org/10.1016/j.injury.2023.111080
Accepted 26 September 2023
Available online 30 September 2023

determining fractures at risk of nonunion as early as possible. Consequently, it is crucial to devise innovative diagnostic approaches with the capacity to forecast fracture healing outcomes and concurrently determine the effectiveness of transformative therapies during the incipient phases of the healing process.

The temporal monitoring of fracture site stiffness or compliance has exhibited efficacy as a reliable predictor of fracture healing outcomes [8–18]. In fracture healing terminology, 'stiffness' characterizes the bone's resistance to deformation under load. Conversely, 'compliance' signifies the inverse, representing how easily the bone can deform. Further, mechanical monitoring methods can provide earlier indications of healing progress compared to radiographic techniques because measurable changes in fracture callus stiffness occur prior to radiographically visible mineralization. Thus, our group has developed a noninvasive radio frequency-based direct electromagnetic coupling (DEC) approach that quantifies the bending stiffness of fractures stabilized by any clinically available implant, such as intramedullary nails (IMN) or plates, to predict the temporal bone healing cascade. In essence, the external telemetric DEC antennas produce a non-ionizing electromagnetic field, establishing electromagnetic coupling with the fractured bone and/or implanted hardware situated in its proximal-spatial domain [19–21]. The resultant "echo" apparent resonant frequency (ARF) oscillates with the varying interstitial distance between the coupled constituents, enabling micron-resolution (μm) defection measurements of the construct. Ergo, analyzing ARF shifts during controlled mechanical loading applications such as bending provides a noninvasive technique to directly measure the stiffness and/or compliance of fractures. Periodic DEC evaluations can thus signal whether proper healing progression is underway, as evidenced by the temporally increasing fracture stiffness, or if healing progression has decelerated or ceased, as indicated by invariant fracture stiffness. Prior works by our group have [1] established the electromagnetic foundations of the DEC technique via computational models [20,22] experimentally demonstrated the efficacy of the DEC technique to monitor changes in stiffness using in vitro fracture healing models [19,23] utilized DEC to distinguish between normal and delayed healing in a large animal fracture model [21], and [4] demonstrated clinical feasibility of the DEC technique to monitor tibial fracture healing in an observational clinical patient study in both an in-clinic and at-home telemedicine settings.

Previous versions of the DEC method utilized a coiled antenna design, which exhibited a nonlinear sensitivity at significantly large implant deformations. This required the initial gap between the coiled antenna and the implant to be precisely adjusted for each patient and experimental iteration [21]. The coiled antenna DEC system primarily reported the temporal rate of change in antenna sensitivity in MHz shift per week to indicate the healing progression [21]. While this rate of change (MHz/Week) scale offered meaningful insights into the healing process, its clinical interpretability was limited. In response to these challenges, the recent introduction of a miniaturized Vivaldi antenna marks a significant advancement in the DEC technology. This design offers the dual advantage of a much-reduced antenna size without compromising antenna sensitivity [20]. The small size and reduced antenna crosstalk of the Vivaldi antennas enable a multi-antenna array DEC system (maDEC) that can more precisely determine fracture site stiffness using multiple measurements along the length of a fractured bone. Further, the development and implementation of a rapid (<60 s) calibration technique after each testing session enable the straightforward determination of fracture site bending stiffness (Nm/deg) or compliance (deg/Nm) from the reported ARF data [20]. These easily interpretable output metrics offer a direct and clinically relevant measure of the progression of bone fracture healing.

However, to fully determine the extent of the clinical relevance of these advancements during the critically crucial acute healing period, further translational *in vivo* studies were required. Thus, the primary objective of this study was to evaluate the effectiveness of the miniaturized Vivaldi antenna array in predicting the changes in stiffness during the acute healing of bone fractures in an ovine model (union vs. nonunion). Moreover, this study also compared these outcomes with tissue-level healing metrics at two sacrifice periods during the acute healing phase. These comparisons aimed to establish a correlation between the healing predictions provided by the maDEC system and the actual tissue-level changes that occur during the healing process, thereby validating the utility of this novel system in monitoring and potentially guiding fracture healing treatment.

In pursuit of these objectives, we employed a three-antenna maDEC system within an ovine animal model of IMN-stabilized fractures to assess healing outcomes across two acute sacrifice time points. We hypothesize that the proposed maDEC approach could non-invasively indicate the temporal evolution of fracture stiffness as a measure of healing and that maDEC data would correlate with tissue-level changes observed at the time of sacrifice.

Methods

Study overview

The efficacy of the maDEC system was assessed using a unilateral ovine metatarsal ostectomy fracture model [24–27] stabilized with intramedullary nailing (IMN; 8 mm x 147 mm, Biomedtrics, I-Loc Fixator, Whippany, NJ) in a total of 12 skeletally mature (≥3 years old) Columbia-Rambouillet ewes (Fig. 1). Animals were divided into two treatment groups, each comprising six individuals. In one group (normal), the animals underwent a 3 mm mid-metatarsal ostectomy, expecting to approach bony union at the 8-week mark post-surgery. The second group (impaired) experienced a more significant 10 mm mid-metatarsal ostectomy. It was anticipated to demonstrate a deficient healing pathway, potentially resulting in a delayed union or non-union at the 8-week sacrifice time. Three animals from each group were euthanized at 4- and 8-week intervals, with all animals included in the subsequent analyses detailed below. Due to the visibly distinct difference in ostectomy size between treatment groups, as evident in radiographs and histology samples, researchers were not blinded to the treatment. The Colorado State University Institutional Animal Care and Use Committee (IACUC) approved the study protocol (CSU#1038).

In vivo maDEC measurements

In vivo maDEC measurements were conducted twice a week from one to four weeks post-surgery and once a week after that until sacrifice. The test subjects were mildly sedated using isoflurane anesthesia to ensure easier animal handling during limb testing and radiographic imaging. The ewes were positioned in lateral recumbency, and the metatarsus undergoing treatment was placed in a four-point bending frame (Fig. 2a). The fixture's configuration was such that the outer contact points spanned the entire metatarsal length (150 mm), extending beyond the ostectomy. Meanwhile, the inner contact points, with a span of 38 mm, were situated just inside the outer points, closely flanking the ostectomy site. This arrangement guaranteed a concentrated pure bending moment at the ostectomy site. The bending moment was induced by modulating the contact force of the inner bending contact points. Contact force was measured at 100 Hz via load cell (Model 53; Honeywell; Charlotte, NC) and converted to maximum bending moment (N-m) according to the fixture geometry.

Five non-destructive, quasi-static pure moment load and unload cycles, generating moments ranging between 1.1–3.4 N-m, were applied at 0.05 Hz. Five distinct data collection trials were conducted per testing day to simulate a more authentic clinical situation - where patients might place their limb differently in the maDEC testing system for each session. For each trial, the metatarsus was removed from and then repositioned in the loading frame. The mean and standard deviation data from the maDEC trials were calculated from a single testing day,

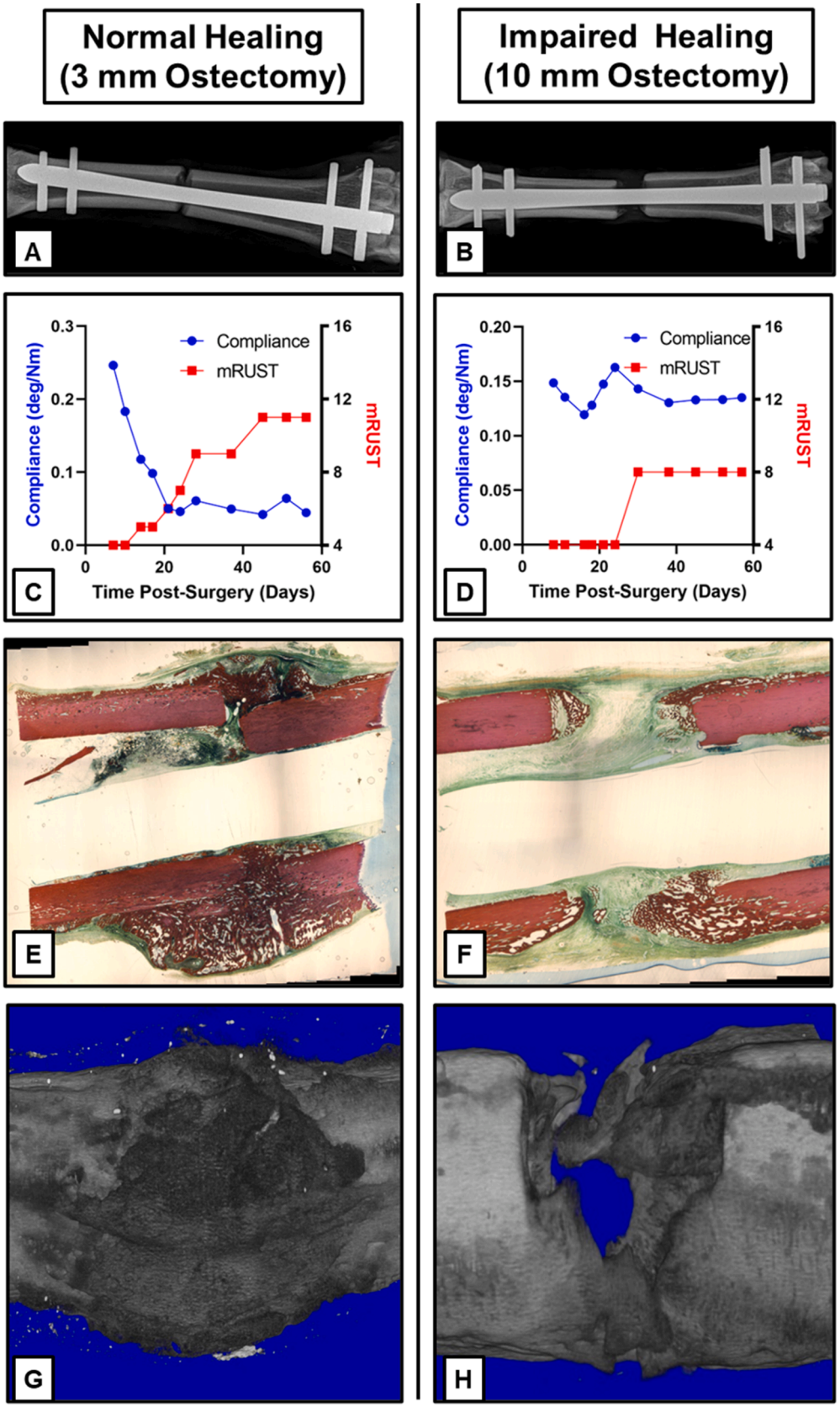

Fig. 1. Study Overview – Representative images of post-surgical radiographs (A,B), *in vivo* temporal maDEC-measured bending compliance data overlaid with mRUST scores (C,D), 8-week post-sacrifice sagittal H&E histology sections (E,F), and μCT reconstructions (G,H) for the normal healing and impaired healing groups respectively.

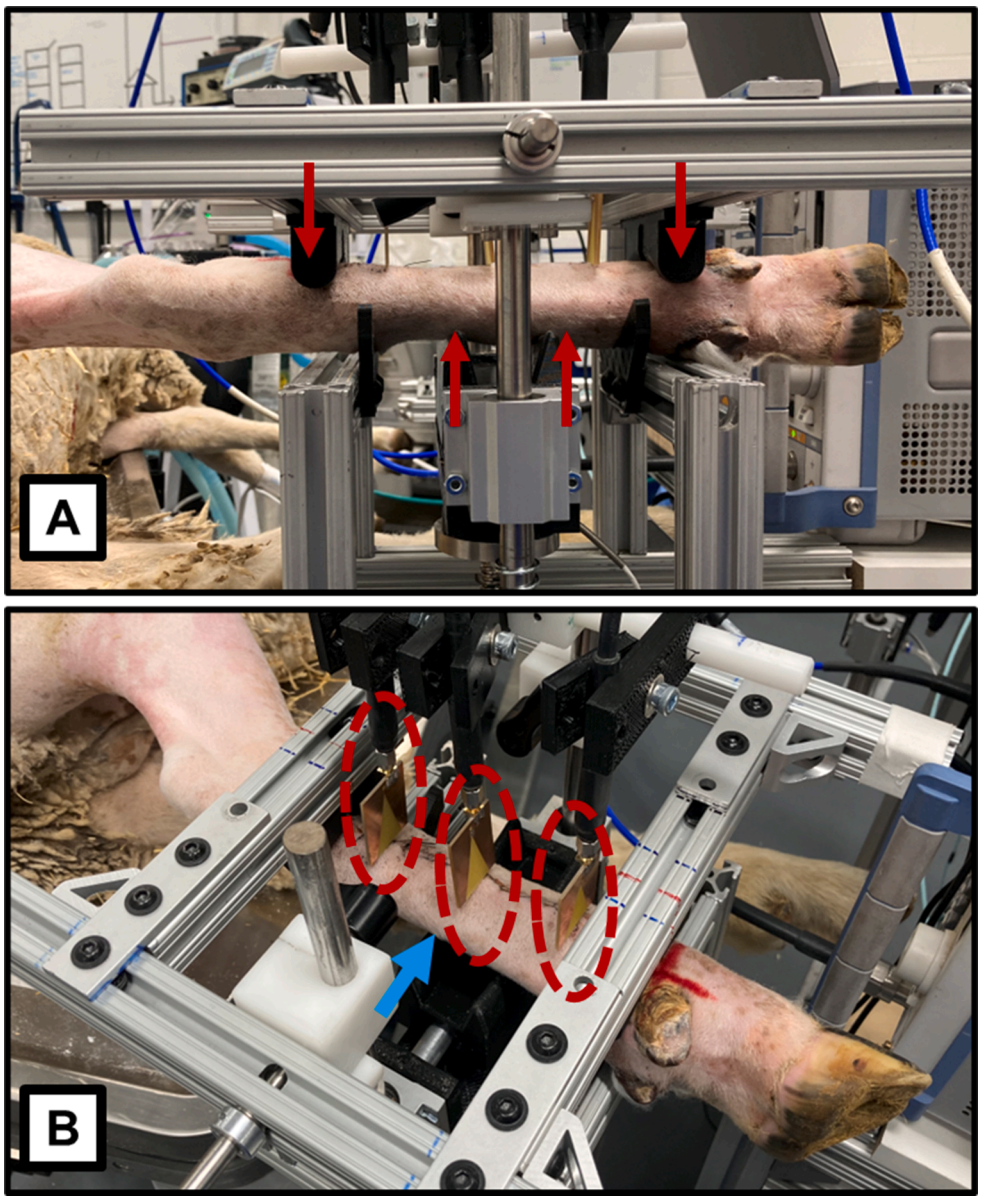

Fig. 2. (A) An ovine metatarsus in the maDEC system with the fracture site (blue arrow) centered below the Vivaldi antenna array (red circles). (B) Lateral view of the maDEC system's 4-point bending setup (red arrows) that apply a pure moment across the fracture.

thereby measuring the system's repeatability.

A three-antenna array was used, in which one antenna each was set to be located above the midspan of the proximal and distal native bone segments, and one antenna was positioned above the middle of the ostectomy (Fig. 2b). The distance between the skin and the antennas was not explicitly set, ranging from 0.5–5 mm depending on post-surgical tissue swelling and animal girth. Each DEC antenna's coupled RF resonant frequency was measured as previously described [20,22,23], and each antenna in the array was calibrated following each test to enable the direct conversion of the RF resonant frequency data to construct deflection (μm) [20]. The deformation of the metatarsus-IMN construct, expressed in microns, was recorded by each antenna under the applied maximum bending moment. The angular displacement at the fracture site, given in degrees, was computed based on the deflection data gathered from the three antennas. This angular change was determined by comparing the unloaded and loaded positions, expressing changes at the mid-point antenna (i.e., at the ostectomy) relative to the average of the proximal and distal antennas. The average bending compliance (Deg./N-m) of the metatarsus-IMN construct was determined as the slope of the angular displacement versus the bending moment curve, providing a measure of the construct's stiffness. The mean bending compliance was calculated for all loading cycles and testing repetitions for each testing session. These average compliance data were monitored over the initial 4-week healing period for all samples to determine the compliance rate of change (i.e., the slope of the compliance data over time; Deg./N-m/week) for each animal (Fig. 3). The cumulative normalized stiffness parameter was defined as the maDEC-reported stiffness, normalized to the first measurement, and integrated over the course of data collection until the time of sacrifice. This parameter was designed to capture the relative change in the accumulation of maDEC-reported bending stiffness throughout the entirety of the healing process for all samples, regardless of the sacrifice period.

Radiographic analysis

Given that our central operating tenet is based upon the concept that the proposed maDEC approach can determine the course of early bone healing before radiographic techniques become clinically useful,

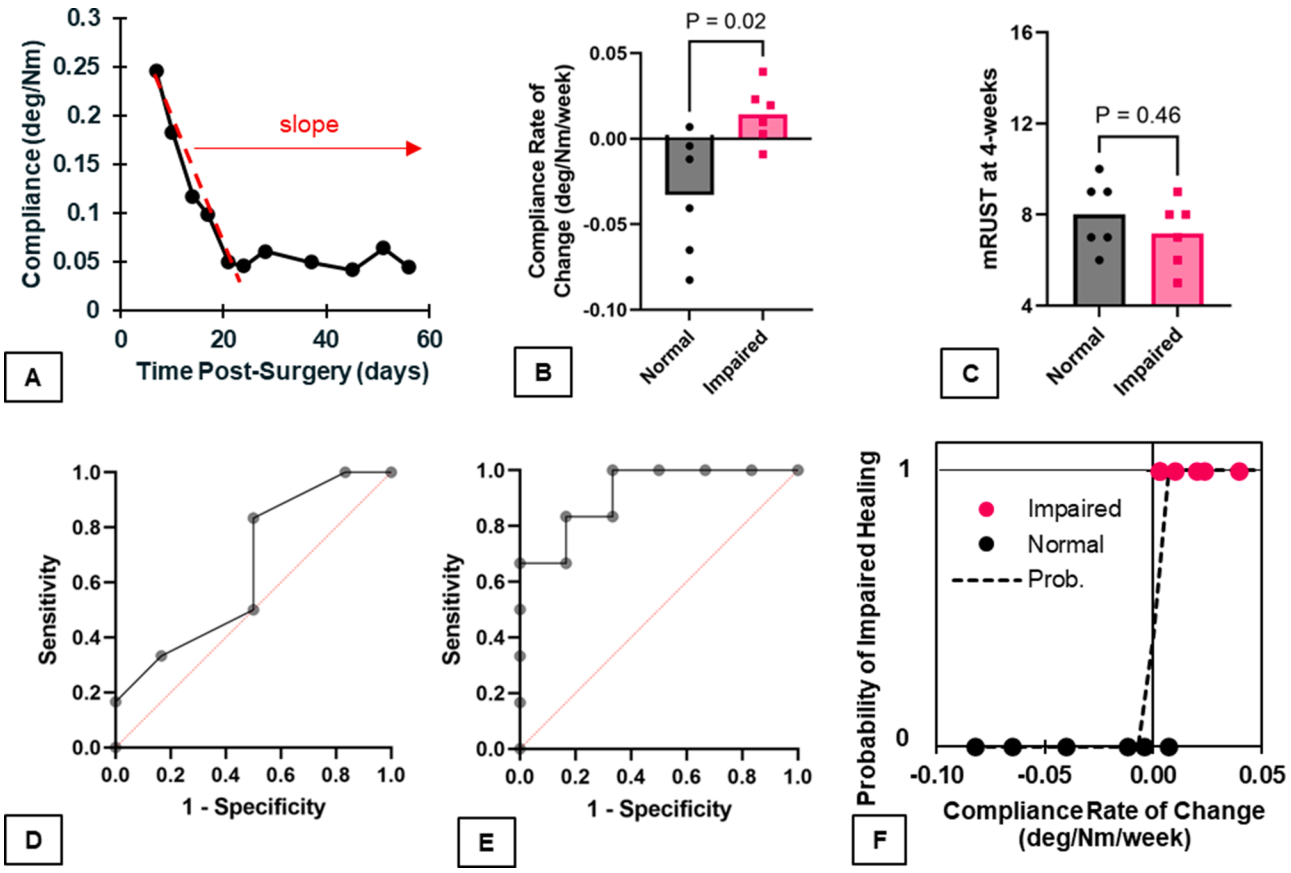

Fig. 3. (**A**) The compliance rate of change was measured as the slope of the maDEC compliance vs. days post-surgery during the initial 4 weeks of healing, and (**B**) this metric was significantly different between healing groups ($p = 0.02$). (**C**) The mRUST scores at four weeks were not significantly different between healing groups ($p = 0.46$). A logistical regression assessed the specificity and sensitivity of maDEC and mRUST approaches to predict impaired healing. (**D**) The mRUST receiver operating characteristic (ROC) demonstrated decreased specificity and sensitivity as a predictor of impaired healing resulting in an area under (AUC) of the ROC curve of 0.65. (**E**) The maDEC ROC demonstrated increased specificity and sensitivity as a predictor of impaired healing resulting in an AUC of the ROC curve of 0.92. (**F**) The maDEC probability curves demonstrated that the compliance rate of change has a high probability of predicting impaired healing during acute fracture healing.

anterior-posterior (AP) and lateral plane radiographs were taken. These digital images were analyzed with respect to the degree of callous formation, mineralization in the fracture gaps, and degree of bridging bone. Biplanar radiographs (CXDI-60 G, Universal Imaging, New York) were obtained at the same measurement intervals as in vivo maDEC measurements. The modified radiographic union score for the tibia (mRUST) system, which assigns a score ranging from 4 (no bone bridging at each of the cortices) to 16 (connected bone bridging at each of the cortices), was used to grade each set of radiographs [28–30]. The scoring was carried out by a board-certified veterinary surgeon (HS). Despite the subjective nature of radiograph interpretation when evaluating fracture healing in clinical practice [28,31–34], the mRUST grading system remains a gold standard for clinical fracture assessment. It was thus employed to directly compare maDEC bending compliance data to radiographic evidence of bony healing.

Ex vivo analyses

Following euthanasia, the surgically treated metatarsus was subjected to μCT, destructive biomechanical four-point bending, and histomorphometry. The biomechanical tests and μCT scans were performed within four hours of the sacrifice. Detailed methodologies of the *ex vivo* analyses are provided in the supplemental materials.

In brief, extraneous soft tissues and the intramedullary nail (IMN) were removed while leaving the fracture callus intact. The metatarsus was then scanned (Scanco micro-CT 80, Scanco USA Inc., Wayne, PA) at a 51 μm voxel size resolution to determine the fracture site's bone volume and density parameters (Figure S1).

After μCT scanning, the treated and the contralateral metatarsi were subjected to quasi-static four-point bending until failure (MTS Systems Corporation, Eden Prairie, MN) (Figure S2). The testing was halted immediately upon observing yielding failure before the bone experienced a catastrophic failure. This approach allowed for the measurement of the ultimate failure moment while preserving the specimen for subsequent histomorphometry analysis.

Finally, the samples were prepared for plastic histology using standard procedures [35,36]. Two slides per sample were prepared in the sagittal plane, ensuring they included the fracture defect and the surrounding callus region (Figure S3). Bone area fraction (%), soft tissue area fraction (%), and the total new bone area (mm^2) were calculated at the fracture.

Statistical analysis

Engineers with statistical experience in preclinical studies (KL and KM) executed statistical analysis in which the significance threshold was set at $\alpha = 0.05$ (Prism 9.5.1, GraphPad Software, Boston, MA, USA), and power analyses were performed (R-Studio Build 421, PBC, Boston, MA).

A Welch's *t*-test was utilized to assess the efficacy of the maDEC system in distinguishing differences in the reported compliance rate of change between the normal healing and impaired healing groups.

The mRUST scores, which are ordinal data, were not assumed to be

normally distributed or meet the other assumptions necessary for a Welch's *t*-test. Therefore, the Mann-Whitney U test was employed to compare the mRUST scores between the normal and impaired healing groups.

A two-way ANOVA with Tukey multiple comparisons was employed for all post-sacrifice outcome parameters to compare the normal and impaired healing groups at the 4-week and 8-week time points. Logarithmic transformations were applied for data sets that did not satisfy the assumptions of normality and equal variance.

Linear regression analysis was conducted to assess the correlations between *in vivo* maDEC stiffness on the day of sacrifice, the rate of change in compliance during healing, and the cumulative normalized stiffness data with the post-sacrifice biomechanical, μCT, and histomorphometric outcome measures. R-squared values were calculated for each correlation to assess the strength and direction of the relationship between the investigated variables. There are no set standards for interpreting the power of R^2 in its application to clinical relevance [37], and even a low R^2 can offer valuable insights about data trends in a clinical model, although it may lack precision [38]. Therefore, all correlations were reported regardless of the r-squared value.

Logistic regression was utilized on the maDEC compliance rate of change and mRUST data, individually and in combination. This evaluation predetermined the treatment category - either normal or impaired - as a binary parameter. Together with the corresponding areas under the receiver operating characteristic (ROC) curves [39,40], this analysis estimated the probability, sensitivity, and specificity of the three approaches: maDEC alone, RUST alone, and the combination of maDEC and mRUST. The ROC curve was used to assess a test's overall diagnostic performance and compare the performance of two or more diagnostic tests. It can also be used to select an optimal cut-off value for determining the presence or absence of impaired healing [40]. The Area Under the Curve (AUC) of the ROC was also calculated as it is a widely used measure to evaluate the accuracy of diagnostic tests [40]. The AUC can range from 0.5 (no better than random prediction) to 1.0 (perfect prediction). Thus, an ideal ROC curve, indicating excellent sensitivity and specificity, would have an AUC of 1.0.

Results

In vivo assessments

Fig. 3 contrasts the maDEC compliance rate of change over the initial four-week healing phase with the mRUST scores. While mRUST scores showed no marked variation between healing groups, the maDEC approach revealed a distinct difference and demonstrated superior specificity and sensitivity in predicting impaired healing, as evidenced by its ROC AUC value. Specifically, in the normal healing group, maDEC compliance data demonstrated a decreasing trend during the acute healing phase, indicative of increased mechanical stiffness at the fracture site (Figs. 1C, 3B). Conversely, throughout the study, the impaired healing group exhibited a temporally static or even increasing trend in maDEC-reported fracture site compliance (Figs. 1D, 3B). In particular, the rate of change in the maDEC-measured bending compliance during the first four weeks and over the total healing period showed significant differences between the normal and impaired healing groups ($P = 0.02$ and $P = 0.04$, respectively). In contrast, radiographically derived mRUST healing measures did not significantly differ between the groups ($P = 0.46$) (Fig. 3C). This lack of significance in the radiographic mRUST data between the two models underscores the lack of specificity and sensitivity in radiographic data during the acute healing phase (Fig. 3D).

The logistic regression analysis revealed that the maDEC compliance rate of change data was a superior predictor of healing outcomes compared to the mRUST score (Fig. 3B–E). The predictive capacity improved only slightly (+0.02 in the AUC) and not significantly ($P = 0.78$) when the maDEC compliance rate of change and mRUST were combined in a multivariate logistic regression model compared to maDEC alone. Specifically, the areas under (AUC) the ROC curves for mRUST, the maDEC reported compliance rate of change, and the combined mRUST and compliance rate of change as predictors were 0.65, 0.92, and 0.94, respectively. These data indicate that maDEC data had the greatest sensitivity and specificity for a single diagnostic approach (Figure D, E). The maDEC reported a compliance rate of change also demonstrated a high probability of predicant impaired healing (Fig. 3F)

Post sacrifice correlations

The supplemental material document details biomechanical, μCT, and histological findings. These data demonstrated that the chosen sacrifice times of 4 and 8 weeks led to statistically significant differential temporal healing responses (Figures S1, S2, and S3). These data, in part, also demonstrate that the sacrifice time points captured an acute healing time frame for this fracture model. For example, the biomechanical data showed that the ultimate failure moment of metatarsi in the normal osteometry (i.e., 3 mm) group was 22.9 ± 15.7 Nm (mean ± standard deviation) at the 8-week timepoint (Figure S2). However, this mean was only 14 % of the mean ultimate failure moment for healthy contralateral metatarsi (169 ± 24 Nm). Similar structural and cellular indicators of acute healing can be observed in the μCt (Figures S1) and histological (Figures S3) data.

Most importantly, these data enabled correlations between maDEC data gathered at the time of sacrifice and subsequent post-sacrifice analysis, providing insights into the maDEC approach to correlate with tissue-level alterations at the fracture site indirectly. Fig. 4 displays the linear regression of maDEC stiffness data against ex vivo outcomes, highlighting significant correlations ($p \leq 0.05$ and power > 0.80). Detailed statistical power for each correlation can be found in Table 1. These scatterplots represent correlations between the *in vivo* maDEC data recorded at the time of sacrifice or throughout the entire data collection period, and *ex vivo* biomechanics, μCT, and histomorphometry outcomes were generated (Fig. 4). These correlations were assessed for their r-squared correlation and statistical significance, and the corresponding statistical powers are provided in Table 1. Note that in some comparisons, the statistical power is below the conventionally accepted value of 0.8, which suggests a higher risk of Type II error (i.e., failing to detect a difference where one exists). Conversely, other comparisons display appropriate statistical power, thus lowering the risk of Type II error. Therefore, while some results should be interpreted cautiously due to low power, we consider our approach suitable for this study's exploratory and methodological nature.

Several notable correlations ($p \leq 0.05$) with statistical power above 0.8 were identified. Notably, the maDEC cumulative normalized stiffness displayed correlations with all outcome parameters. These parameters included ultimate failure load (N-m), bone volume / total volume (BV/TV), mean bone density of total volume (MDVT; mm Hg/cm^3), bone area fraction within the cortical region of Interest (ROI), and total new bone area (mm^3) (Table 1 and Fig. 4). Taking into account the r-squared values, statistical power, and p-values for these correlations, the data suggest that the maDEC cumulative normalized stiffness had the highest strongest correlations in indirectly reflecting the fracture site's biomechanical ultimate failure load ($r^2 = 0.8$, power = 1.0, and $p < 0.001$), as well as the histologic total new bone area ($r^2 = 0.78$, power = 0.99, and $p < 0.001$). The other correlations had r-squared values of approximately 0.6, pointing to slightly lower sensitivity. Despite these variations, the correlations collectively illustrate the maDEC system's potential to capture several pivotal aspects of the tissue-level fracture healing process. This holds regardless of the fracture model used or the time at which the animal was sacrificed, emphasizing the robustness and versatility of the maDEC system when used temporally.

The relative bone and soft tissue area fractions reveal that, at the 4-week timepoint, there was a much more significant fraction of soft tissue in both ROIs (about 60–80 %), while the bone fraction was about 10–25 % for normal healing and 5–10 % for impaired healing. Notably, the *in*

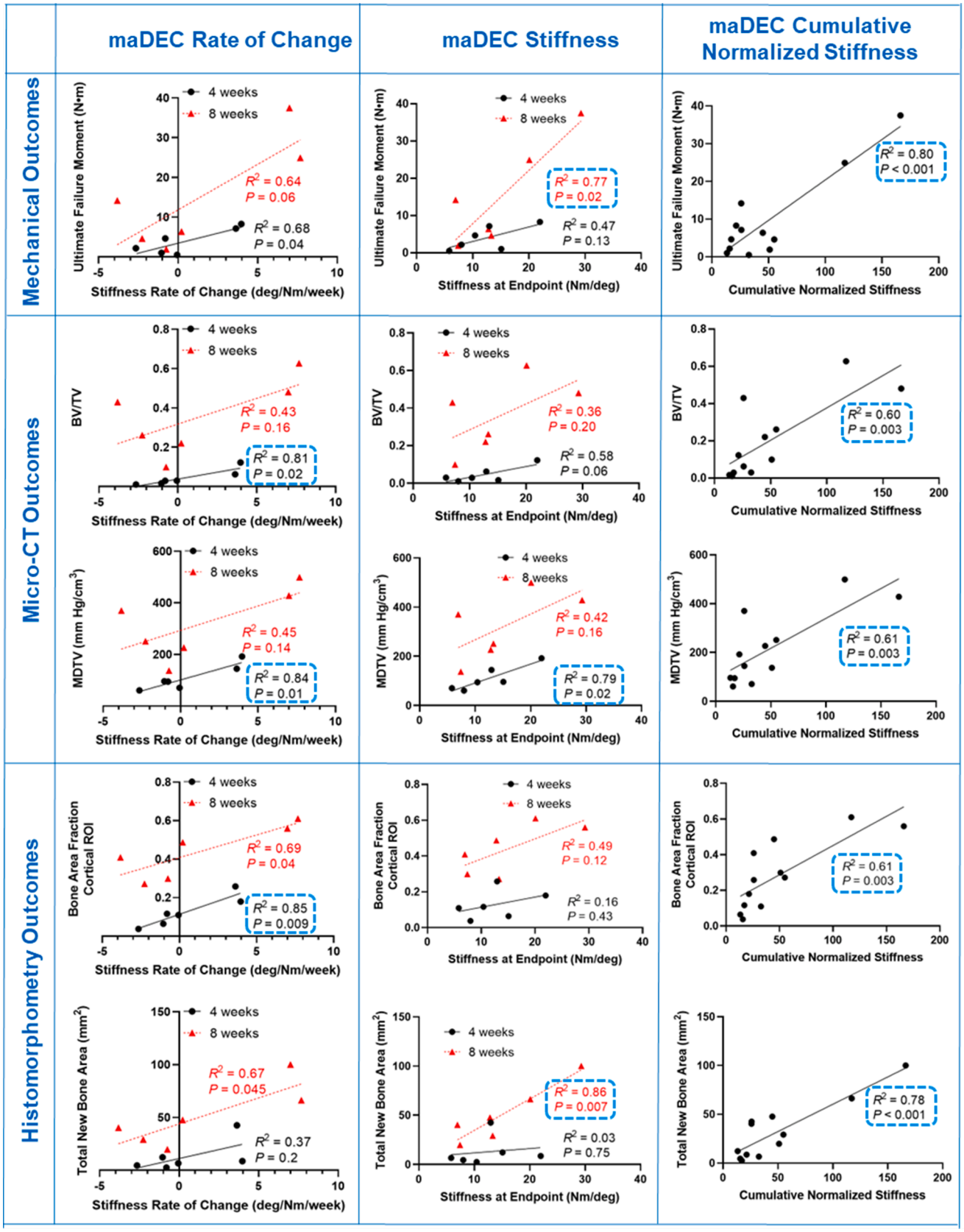

Fig. 4. Linear regression results of maDEC reported stiffness data correlated to *ex vivo* outcome parameters. R-squared and p-values are given in each panel. Statical power for each correlation is given in Table 1. Correlations with p-values ≤ 0.05 and power above 0.80 have been highlighted with blue boxes.

Table 1
Statistical summary for all analyses showing power for each statical test or correlation.

Data	Statistical test	Comparison	Time point	Samples (N)	R^2	Statistical power	Test type
maDEC	Welches T-test	Normal vs. Impaired	4-week	3 vs 3	–	0.48	Parametric
maDEC	Welches T-test	Normal vs. Impaired	8-week	3 vs 3	–	**0.90**	Parametric
mRUST	Mann–Whitney *U* test	Normal vs. Impaired	4-week	3vs 3	–	n/a	Nonparametric / Ranked
mRUST	Mann–Whitney *U* test	Normal vs. Impaired	8-week	3 vs 3	–	n/a	Nonparametric / Ranked
maDEC vs. Biomechanical	Linear regression analysis	Stiffness Rate of Change vs. Failure Moment	4-week	6	0.68	0.76	Parametric
maDEC vs. Biomechanical	Linear regression analysis	Stiffness Rate of Change vs. Failure Moment	8-week	6	0.64	0.69	Parametric
maDEC vs. Biomechanical	Linear regression analysis	Stiffness @ Sacrifice vs. Failure Moment	4-week	6	0.47	0.42	Parametric
maDEC vs. Biomechanical	Linear regression analysis	Stiffness @ Sacrifice vs. Failure Moment	8-week	6	0.77	**0.91**	Parametric
maDEC vs. Biomechanical	Linear regression analysis	Cumulative Normalized Stiffness vs. Failure Moment	4 and 8-week	12	0.80	**1.00**	Parametric
maDEC vs. μCT	Linear regression analysis	Stiffness Rate of Change vs. BV/TV	4-week	6	0.81	**0.96**	Parametric
maDEC vs. μCT	Linear regression analysis	Stiffness Rate of Change vs. BV/TV	8-week	6	0.43	0.37	Parametric
maDEC vs. μCT	Linear regression analysis	Stiffness @ Sacrifice vs. BV/TV	4-week	6	0.58	0.59	Parametric
maDEC vs. μCT	Linear regression analysis	Stiffness @ Sacrifice vs. BV/TV	8-week	6	0.36	0.29	Parametric
maDEC vs. μCT	Linear regression analysis	Cumulative Normalized Stiffness vs. BV/TV	4 and 8-week	12	0.60	**0.97**	Parametric
maDEC vs. μCT	Linear regression analysis	Stiffness Rate of Change vs. MDTV	4-week	6	0.84	**0.98**	Parametric
maDEC vs. μCT	Linear regression analysis	Stiffness Rate of Change vs. MDTV	8-week	6	0.45	0.40	Parametric
maDEC vs. μCT	Linear regression analysis	Stiffness @ Sacrifice vs. MDTV	4-week	6	0.79	**0.94**	Parametric
maDEC vs. μCT	Linear regression analysis	Stiffness @ Sacrifice vs. MDTV	8-week	6	0.42	0.36	Parametric
maDEC vs. μCT	Linear regression analysis	Cumulative Normalized Stiffness vs. MDTV	4 and 8-week	12	0.61	**0.97**	Parametric
maDEC vs. Histomorphometry	Linear regression analysis	Stiffness Rate of Change vs. Bone Area Fraction Cortical ROI	4-week	6	0.85	**0.99**	Parametric
maDEC vs. Histomorphometry	Linear regression analysis	Stiffness Rate of Change vs. Bone Area Fraction Cortical ROI	8-week	6	0.69	0.78	Parametric
maDEC vs. Histomorphometry	Linear regression analysis	Stiffness @ Sacrifice vs. Bone Area Fraction Cortical ROI	4-week	6	0.16	0.13	Parametric
maDEC vs. Histomorphometry	Linear regression analysis	Stiffness @ Sacrifice vs. Bone Area Fraction Cortical ROI	8-week	6	0.49	0.45	Parametric
maDEC vs. Histomorphometry	Linear regression analysis	Cumulative Normalized Stiffness vs. Bone Area Fraction Cortical ROI	4 and 8-week	12	0.61	**0.97**	Parametric
maDEC vs. Histomorphometry	Linear regression analysis	Stiffness Rate of Change vs. Total New Bone Area	4-week	6	0.37	0.30	Parametric
maDEC vs. Histomorphometry	Linear regression analysis	Stiffness Rate of Change vs. Total New Bone Area	8-week	6	0.67	0.74	Parametric
maDEC vs. Histomorphometry	Linear regression analysis	Stiffness @ Sacrifice vs. Total New Bone Area	4-week	6	0.03	0.06	Parametric
maDEC vs. Histomorphometry	Linear regression analysis	Stiffness @ Sacrifice vs. Total New Bone Area	8-week	6	0.86	**0.99**	Parametric
maDEC vs. Histomorphometry	Linear regression analysis	Cumulative Normalized Stiffness vs. Total New Bone Area	4 and 8-week	12	0.78	**1.00**	Parametric

vivo maDEC bending compliance data showed a significant distinction between normal and impaired healing at this 4-week time when the fracture callus consisted primarily of soft tissue (Figure S3).

The maDEC data collected during sacrifice demonstrated a limited number of statistically significant and statistically powered correlations with post-sacrifice measurements (Table 1 and Fig. 4). The maDEC data at the time of sacrifice correlated with μCT and histological measurements of new bone in 50 % of the analyses performed for the 4-week time point and in only 12.5 % of the analyses at the 8-week time point.

Furthermore, only maDEC stiffness correlated with ultimate failure moment, with the rate of change in maDEC-reported stiffness trending towards significance ($p = 0.06$) at the 8-week period. These findings underscore that individual maDEC measurements may not be as effective as ongoing temporal monitoring throughout the healing period, as represented by metrics such as cumulative normalized stiffness.

Discussion

This study aimed to utilize a newly developed Vivaldi antenna array, accompanied by a unique calibration procedure, in an *in vivo* setting. The specific goal was to explore the correlation between the data reported by this multi-antenna direct electromagnetic coupling (maDEC) system and tissue-level changes that occur during the acute phase of bone healing. Our overarching goal was to generate proof-of-concept data to evaluate if the maDEC approach could potentially be adapted to guide clinical decision-making processes, such as determining the appropriate timing for weight-bearing resumption, surgical revisions, and the administration of therapeutics.

Previous studies have shown that radiographic evaluations of bone fracture healing are subjective and inaccurate [41], and there is a poor correlation between the radiographic measurements of callus amount and the healed bone stiffness [42]. Opportunely, this investigation, along with comparable methodologies [11–13,16,43–49], has exhibited notable success in utilizing temporal changes in fracture site compliance data to signify the healing trajectory. Fracture site compliance constitutes an unequivocal quantitative measure obtainable and interpretable at any juncture throughout the healing cascade, offering an objective indication of healing progress. For instance, it has been demonstrated that a human fracture stiffness magnitude of 15 N-m/degree serves as an efficacious benchmark for diagnosing fracture union [50,51], and temporal alterations in fracture stiffness can foresee healing outcomes a minimum of 2.5 weeks ahead of radiographic diagnosis [52]. By monitoring compliance at the fracture site, clinicians and engineers can observe the changes in the mechanical environment and adjust treatment strategies accordingly. This is particularly important for the development of personalized and adaptive treatment plans.

The results presented in this study are consistent with previous DEC research for evaluating the ability of this technology to measure implant deflections at the micron level and employ this information to directly ascertain disparities in fracture site compliance as an indicator of temporal osseous healing [20,22,23]. A multi-antenna DEC approach has been previously investigated using coiled antenna configurations, showcasing the capacity to obtain independent assessments of distinct spatial areas [21]. However, the Vivaldi antennas [20] employed in this study for non-contact sensing offer several significant benefits over coiled antennas, such as (1) a compact antenna design that enables the placement of multiple antennas in very close proximity without interference, (2) improved radio frequency (RF) and displacement sensing accuracy, and (3) an enhanced linear relationship between the RF resonant frequency and implant deflections across a larger initial gap between the implant and the antenna. Consequently, the multi-antenna DEC (maDEC) technique represents a substantial advancement in this technology platform. As this study calculated angular displacement with three antennas, we conclude that these data demonstrate that the maDEC's approach could be capable of determining localized fracture site compliance at multiple positions within a single bone. This approach would signify a fundamental shift in a clinician's capacity to oversee an array of intricate fracture situations encompassing multi-fragmented comminuted fractures or allograft incorporation instances.

Furthermore, this research demonstrated statistically significant associations between the temporal maDEC cumulative normalized stiffness data and tissue-level responses at the fracture location, encompassing biomechanical, structural (as assessed by μCT), and compositional (as evaluated by histomorphometry) alterations transpiring during the acute timeframe. In conjunction with the presented probability and ROC AUC findings, these correlations with tissue-level modifications suggest that maDEC data can predict the fracture healing cascade and provide meaningful insights into the strength and architecture at the fracture site throughout the acute temporal healing process. These correlations are important, as understanding the temporal tissue changes observed during fracture healing is essential for optimizing patient care, developing personalized treatment plans, advancing therapeutic strategies, and evaluating treatment efficacy. This knowledge can potentially improve patient outcomes and enable new possibilities in fracture management.

The ovine model of metatarsal fracture, which was employed to assess the effectiveness of maDEC technology, shares similarities with human diaphyseal long bone fractures. Nevertheless, it is essential to note that this model has certain limitations. The impaired healing method of utilizing a large defect had the desired outcome of causing a delayed healing response. Still, it did not prevent callus formation, and it is unknown if bony union would have occurred if animals had survived for a more extended period. While this model provided an appropriate platform for assessing the maDEC method, the results do not necessarily represent all pathological impairments to fracture healing. Also, the mRUST scores in this large defect model may not represent clinical fractures; however, based on a parametric finite element study, we expect this model to be an accurate biomechanical platform for assessing the DEC approach [19]. This likely means that surgical treatment groups predetermine our outcomes in the logistic regression (prediction) analysis. Further, while the overall trends in maDEC results are translatable to human fractures, bony healing rates can differ between ovine and human species.

These data observations suggest that the real power of approaches that track *in vivo* compliance or stiffness, like the maDEC, to predict healing lies in their ability to track changes over time rather than providing one-time measurements. The cumulative normalized stiffness, which integrates measurements over the entire healing period, appeared to give a more accurate reflection of the healing process and correlates more strongly with other outcome measures. Thus, using maDEC and similar approaches in clinical or research settings may be most beneficial when measurements are taken frequently and monitored longitudinally throughout the healing process.

In summary, to address the shortcomings of current diagnostic methods, it is essential to continue to develop innovative approaches akin to the maDEC technology presented herein, capable of predicting fracture healing outcomes and potentially determining the efficacy of transformative therapies during the early phases of the healing process. By incorporating novel diagnostic techniques such as the maDEC approach, clinical and engineering professionals can collaborate to optimize patient care and advance the field of fracture management.

Author disclosures

Kevin M. Labus Ph.D.[1], Declarations of interest: Patent registration, Grant Funding

Jakob Wolynski Ph.D.[1], Declarations of interest: Patent registration

Jeremiah Easley DVM[2], Declarations of interest: None

Holly L. Stewart VMD[2], Ph.D.[2], Declarations of interest: None

Milan Ilic Ph.D.[3], Declarations of interest: None

Branislav Notaros Ph.D.[4], Declarations of interest: None

Taylor Zagrocki [1], Declarations of interest: None

Christian M. Puttlitz Ph.D.[1], Declarations of interest: Patent registration, Grant Funding

Kirk C. McGilvray Ph.D.[1], Declarations of interest: Patent registration, Grant Funding

Disclosure of funding

This project was supported by the National Institute of Health (NIH) - National Institute of Arthritis and Musculoskeletal and Skin Diseases (NIAMS) (R01AR069734 - "*Early Detection and Prediction of Complex Bone Fracture Healing*") and grant from the State of Colorado Office of Economic Development and International Trade (CTGG1 2020-2697 – "Direct Electromagnetic Coupling for Diagnostic Prediction of Fracture Healing")

Declaration of Competing Interest

None.

Acknowledgement

These technologies are patented in the USA (Paten No: 10,641,664; 10,892,558; 11,402,193)

Supplementary materials

Supplementary material associated with this article can be found, in the online version, at doi:10.1016/j.injury.2023.111080.

References

[1] Antonova E, Le TK, Burge R, Mershon J. Tibia shaft fractures: costly burden of nonunions. BMC Musculoskelet Disord 2013;14:42.
[2] Brinker MR, Hanus BD, Sen M, O'Connor DP. The devastating effects of tibial nonunion on health-related quality of life. J Bone Joint Surg Am Volume 2013;95 (24):2170–6.
[3] Heckman JD, Sarasohn-Kahn J. The economics of treating tibia fractures. The cost of delayed unions. Bulletin 1997;56(1):63–72 (Hospital for Joint Diseases (New York, NY)).
[4] Kanakaris NK, Giannoudis PV. The health economics of the treatment of long-bone non-unions. Injury 2007;38(2):S77–84. Suppl.
[5] Tzioupis C, Giannoudis PV. Prevalence of long-bone non-unions. Injury 2007;38 (Suppl 2):S3–9.
[6] Einhorn TA, Gerstenfeld LC. Fracture healing: mechanisms and interventions. Nat Rev Rheumatol 2015;11(1):45–54.
[7] Hak DJ, Fitzpatrick D, Bishop JA, Marsh JL, Tilp S, Schnettler R, et al. Delayed union and nonunions: epidemiology, clinical issues, and financial aspects. Injury 2014;45(Suppl 2):S3–7.
[8] Wade RH, Moorcroft CI, Thomas PB. Fracture stiffness as a guide to the management of tibial fractures. J Bone Joint Surg Br 2001;83(4):533–5.
[9] Claes LE, Cunningham JL. Monitoring the mechanical properties of healing bone. Clin Orthop Relat Res 2009;467(8):1964–71.
[10] Wehner T, Gruchenberg K, Bindl R, Recknagel S, Steiner M, Ignatius A, et al. Temporal delimitation of the healing phases via monitoring of fracture callus stiffness in rats. J Orthop Res 2014;32(12):1589–95.
[11] Kienast B, Kowald B, Seide K, Aljudaibi M, Faschingbauer M, Juergens C, et al. An electronically instrumented internal fixator for the assessment of bone healing. Bone Joint Res 2016;5(5):191–7.
[12] Seide K, Aljudaibi M, Weinrich N, Kowald B, Jurgens C, Muller J, et al. Telemetric assessment of bone healing with an instrumented internal fixator: a preliminary study. J Bone Joint Surg Br 2012;94(3):398–404.
[13] Wilson DJ, Morgan RL, Hesselden KL, Dodd JR, Janna SW, Fagan MJ. A single-channel telemetric intramedullary nail for in vivo measurement of fracture healing. J Orthop Trauma 2009;23(10):702–9.
[14] Melik R, Perkgoz NK, Unal E, Puttlitz C, Demir HV. Bio-implantable passive on-chip RF-MEMS strain sensing resonators for orthopaedic applications. J Micromech Microeng 2008;18(11).
[15] Tan Y, Zhu J, Ren L. A two-dimensional wireless and passive sensor for stress monitoring. Sensors (Basel) 2019;19(1):135.
[16] McGilvray KC, Unal E, Troyer KL, Santoni BG, Palmer RH, Easley JT, et al. Implantable microelectromechanical sensors for diagnostic monitoring and post-surgical prediction of bone fracture healing. J Orthop Res 2015;33(10):1439–46.
[17] Hente R, Cordey J, Perren SM. In vivo measurement of bending stiffness in fracture healing. Biomed Eng Online 2003;2:8.
[18] Claes L, Grass R, Schmickal T, Kisse B, Eggers C, Gerngross H, et al. Monitoring and healing analysis of 100 tibial shaft fractures. Langenbeck's Arch Surg 2002;387 (3–4):146–52.
[19] Wolynski JG, Ilic MM, Labus KM, Notaros BM, Puttlitz CM, McGilvray KC. Direct electromagnetic coupling to determine diagnostic bone fracture stiffness. Ann Transl Med 2022;10(9):510.
[20] Wolynski JG, Ilic MM, Notaros BM, Labus KM, Puttlitz CM, Mcgilvray KC. Vivaldi antennas for contactless sensing of implant deflections and stiffness for orthopaedic applications. Ieee Access 2022;10:1151–61.
[21] Wolynski JG, Labus KM, Easley JT, Notaros BM, Ilic MM, Puttlitz CM, et al. Diagnostic prediction of ovine fracture healing outcomes via a novel multi-location direct electromagnetic coupling antenna. Ann Transl Med 2021;9(15):1223.
[22] Labus KM, Notaros BM, Ilic MM, Sutherland CJ, Holcomb A, Puttlitz CM. A coaxial dipole antenna for passively sensing object displacement and deflection for orthopaedic applications. IEEE Access 2018;6:68184–94.
[23] Labus KM, Sutherland C, Notaros BM, Ilic MM, Chaus G, Keiser D, et al. Direct electromagnetic coupling for non-invasive measurements of stability in simulated fracture healing. J Orthop Res 2019;37(5):1164–71.
[24] Yang YP, Labus KM, Gadomski BC, Bruyas A, Easley J, Nelson B, et al. Osteoinductive 3D printed scaffold healed 5cm segmental bone defects in the ovine metatarsus. Sci Rep 2021;11(1):6704.
[25] Margolis DS, Figueroa G, Barron Villalobos E, Smith JL, Doane CJ, Gonzales DA, et al. A large segmental mid-diaphyseal femoral defect sheep model: surgical technique. J Invest Surg 2022;35(6):1287–95.
[26] Claes L, Eckert-Hubner K, Augat P. The fracture gap size influences the local vascularization and tissue differentiation in callus healing. Langenbeck's Arch Surg 2003;388(5):316–22.
[27] Augat P, Margevicius K, Simon J, Wolf S, Suger G, Claes L. Local tissue properties in bone healing: influence of size and stability of the osteotomy gap. J Orthop Res 1998;16(4):475–81.
[28] Litrenta J, Tornetta 3rd P, Mehta S, Jones C, O'Toole RV, Bhandari M, et al. Determination of radiographic healing: an assessment of consistency using RUST and modified RUST in metadiaphyseal fractures. J Orthop Trauma 2015;29(11): 516–20.
[29] Cooke ME, Hussein AI, Lybrand KE, Wulff A, Simmons E, Choi JH, et al. Correlation between RUST assessments of fracture healing to structural and biomechanical properties. J Orthop Res 2018;36(3):945–53.
[30] Whelan DB, Bhandari M, Stephen D, Kreder H, McKee MD, Zdero R, et al. Development of the radiographic union score for tibial fractures for the assessment of tibial fracture healing after intramedullary fixation. J Trauma 2010;68(3): 629–32.
[31] Blokhuis TJ, de Bruine JH, Bramer JA, den Boer FC, Bakker FC, Patka P, et al. The reliability of plain radiography in experimental fracture healing. Skeletal Radiol 2001;30(3):151–6.
[32] Cekic E, Alici E, Yesil M. Reliability of the radiographic union score for tibial fractures. Acta Orthop Traumatol Turc 2014;48(5):533–40.
[33] Davis BJ, Roberts PJ, Moorcroft CI, Brown MF, Thomas PB, Wade RH. Reliability of radiographs in defining union of internally fixed fractures. Injury 2004;35(6): 557–61.
[34] Lujan TJ, Madey SM, Fitzpatrick DC, Byrd GD, Sanderson JM, Bottlang M. A computational technique to measure fracture callus in radiographs. J Biomech 2010;43(4):792–5.
[35] Dickson GR. Methods of Calcified Tissue Preparation. Elsevier; 1984764 p.
[36] Islam A, Frisch B. Plastic embedding in routine histology. I: preparation of semi-thin sections of undecalcified marrow cores. Histopathology 1985;9(12):1263–74.
[37] Chicco D., Warrens M.J., Jurman G. The coefficient of determination R-squared is more informative than SMAPE, MAE, MAPE, MSE and RMSE in regression analysis evaluation. Peerj Comput Sci. 2021.
[38] Hamilton DF, Ghert M, Simpson AHRW. Interpreting regression models in clinical outcome studies. Bone Joint Res 2015;4(9):152–3.
[39] Hajian-Tilaki K. Receiver Operating Characteristic (ROC) curve analysis for medical diagnostic test evaluation. Caspian J Intern Med 2013;4(2):627–35.
[40] Nahm FS. Receiver operating characteristic curve: overview and practical use for clinicians. Korean J Anesthesiol 2022;75(1):25–36.
[41] Fisher JS, Kazam JJ, Fufa D, Bartolotta RJ. Radiologic evaluation of fracture healing. Skeletal Radiol 2019;48(3):349–61.
[42] Sano H, Uhthoff HK, Backman DS, Yeadon A. Correlation of radiographic measurements with biomechanical test results. Clin Orthop Relat Res 1999;(368): 271–8.
[43] Fischer WJ, Sauer S, Marschner U, Adolphi B, Wenzel C, Jettkant B, et al. editors. Galfenol resonant sensor for indirect wireless osteosynthesis plate bending measurements. Proc IEEE Sens Conf 2009;2009. Christchurch, Canterbury, New Zealand: IEEE.
[44] Ledet EH, Liddle B, Kradinova K, Harper S. Smart implants in orthopedic surgery, improving patient outcomes: a review. Innov Entrepren Health 2018;5:41–51.
[45] Oess NP, Weisse B, Nelson BJ. Magnetoelastic strain sensor for optimized assessment of bone fracture fixation. IEEE Sens J 2009;9(8):961–8.
[46] Sauer S, Marschner U, Adolphi B, Clasbrummel B, Fischer W-J. Passive wireless resonant galfenol sensor for osteosynthesis plate bending measurement. IEEE Sens J 2012;12(5):1226–33.
[47] Schneider E, Michel MC, Genge M, Zuber K, Ganz R, Perren SM. Loads acting in an intramedullary nail during fracture healing in the human femur. J Biomech 2001; 34(7):849–57.
[48] Tan Y, Hu J, Ren L, Zhu J, Yang J, Liu D. A passive and wireless sensor for bone plate strain monitoring. Sensors (Basel) 2017;17(11):2635.
[49] Wachs RA, Ellstein D, Drazan J, Healey CP, Uhl RL, Connor KA, et al. Elementary implantable force sensor: for smart orthopaedic implants. Adv Biosens Bioelectron 2013;2(4).
[50] Richardson JB, Cunningham JL, Goodship AE, O'Connor BT, Kenwright J. Measuring stiffness can define healing of tibial fractures. J Bone Joint Surg Br 1994;76(3):389–94.
[51] Dwyer JS, Owen PJ, Evans GA, Kuiper JH, Richardson JB. Stiffness measurements to assess healing during leg lengthening. A preliminary report. J Bone Joint Surg Br 1996;78(2):286–9.
[52] McClelland D, Thomas PB, Bancroft G, Moorcraft CI. Fracture healing assessment comparing stiffness measurements using radiographs. Clin Orthop Relat Res 2007; 457:214–9.